doi:10.1016/j.jmb.2005.09.082 J. Mol. Biol. (2005) 354, 578–590

JMB

Available online at www.sciencedirect.com

SCIENCE DIRECT®

ELSEVIER

Crystal Structures of Active LytM

Małgorzata Firczuk[1,2], Artur Mucha[3] and Matthias Bochtler[1,2]*

[1]*International Institute of Molecular and Cell Biology ul. Trojdena 4, 02-109 Warsaw, Poland*

[2]*Max-Planck-Institute for Molecular Cell Biology and Genetics, Pfotenhauerstr. 108, 01309 Dresden, Germany*

[3]*Department of Bioorganic Chemistry, Faculty of Chemistry, Wrocław University of Technology, Wybrzeże Wyspiańskiego 27, 50-370 Wrocław, Poland*

**Corresponding author*

Lysostaphin-type enzymes are metalloendopeptidases that are present in bacteriophages and in bacteria. They share the catalytic domain, but normally contain other domains as well. The well-characterized enzymes in this group are all specific for the pentaglycine crosslinks in the cell walls of some Gram-positive bacterial species. Lysostaphin-type enzymes are synthesized as secreted preproenzymes and require proteolytic activation for maturation. Although lysostaphin, the prototypical peptidase in the group, is widely used as a tool in biotechnology and developed as an antistaphylococcal agent, the detailed structure of this enzyme is unknown. So far, only one lysostaphin-type enzyme, the *Staphylococcus aureus* autolysin LytM, has been crystallized in its full-length, inactive form. Here, we describe the synthesis of a convenient reporter substrate, characterize the metal and pH-dependence of an active LytM fragment, and present its crystal structure in three crystal forms at different pH values that either support or do not support activity. In all structures, we find an extended, long and narrow groove that has the active site at its bottom and is delineated on the sides by the most flexible regions of the molecule. In two cases, the groove is partially filled by a loop of a neighbouring molecule in the crystal. As the loop contains three consecutive glycine residues, this crystal packing effect supports the interpretation that the groove is the substrate-binding cleft. To characterize the substrate-binding mode more closely, a phosphinate analogue of tetraglycine was synthesized. Although tetraglycine is a substrate of the active LytM fragment, the phosphinate analogue turned out to be a very poor inhibitor. Crystals that were grown in its presence contained an L(+)-tartrate molecule from the crystallization buffer and not the phosphinate in the active site.

Keywords: metallopeptidase; peptidoglycan amidase; LytM; structure

Introduction

The lysostaphin-type enzymes, the D-Ala-D-Ala amino- and carboxypeptidases, and sonic hedgehog N-terminal domain are a group of peptidases or putative peptidases known collectively as the LAS enzymes,[1] and are now known to include MepA-like enzymes.[2] LAS enzymes share a core-folding motif, which is a four-stranded antiparallel β-sheet of conserved topology, and the active site architecture, which is organized around a single, divalent metal cation. The metal is pentacoordinated according to a single, recent electron paramagnetic resonance/extended absorption fine structure study on cobalt-substituted VanX,[3] but tetracoordinated according to many independent LAS crystal structures, most of which have been solved at high or very high resolution.[1,4] Three of the four zinc ligands in the crystal structures, two histidine residues and an aspartate residue, are strictly conserved. The metal ligands occur in the context of two short sequence motifs, HX(3,6)D and HXH (EXXH in VanX-type enzymes). Although the first histidine residue of the HXH motif (Glu in VanX-type enzymes) is not a Zn^{2+} ligand, it is also located in a conserved place in the vicinity of the active site Zn^{2+} in all known LAS enzymes. With the exception of the N-domain of sonic hedgehog, for which no substrate has been identified, all known LAS enzymes are peptidoglycan amidases.[1]

Abbreviation used: TLC, thin-layer chromatography.

E-mail address of the corresponding author: mbochtler@iimcb.gov.pl

Some LAS enzymes are produced as active enzymes that do not seem to require post-translational processing for activation. D-Ala-D-Ala carboxypeptidase from *Streptomyces albus* and the D-Ala-D-Ala aminopeptidase VanX are both active as full-length proteins.[5,6] In their crystal structures (PDB accession codes 1LBU and 1R44), the central zinc ion is tetracoordinated and a water molecule is present in the first coordination sphere.[4,7] It is thought that this water molecule takes the place that would be occupied by the carbonyl oxygen atom of the scissile amide bond in a productive enzyme–substrate complex. As D-Ala-D-Ala peptidases, MepA-type enzymes are active as full-length proteins, and as in these peptidases, the crystal structure of *Escherichia coli* MepA has a central tetracoordinated zinc ion (PDB accession code 1U10). However, the first coordination sphere of the zinc ion does not include a water molecule. Details of the crystal structure suggest that the "occluding" residue, histidine 110 in *E. coli* MepA, can be displaced by a substrate, but cannot be removed in a processing step.[2]

Lysostaphin-type enzymes differ from other LAS enzymes, because they are either inactive or only poorly active in their full-length, unprocessed forms and require proteolytic processing for activation. For some lysostaphin-type peptidases, the physiologically relevant processing peptidases have been identified.[8] Despite the pharmaceutical interest in mature lysostaphin as an agent against multidrug-resistant staphylococci,[9] crystal structures for the active forms of lysostaphin-type peptidases are not available. The only lysostaphin-type peptidase that has been crystallized is full-length LytM, which was believed originally to be the active species, but turned out to be a latent form in the light of the crystal structure.[10]

LytM is an autolysin from *Staphylococcus aureus*, which was identified originally in an autolysis-defective mutant strain.[11] The enzyme is specific for glycyl–glycine peptide bonds, which are present in the crosslinking pentapeptides of many *Staphylococcus* species,[12] including *S. aureus*. When the full-length form of the enzyme was crystallized (PDB accession code 1QWY), a two-domain protein was found. The N-terminal domain is not present in many other lysostaphin-type peptidases and its function is not known. The C-terminal domain is the conserved catalytic domain, which turned out to contain a disordered stretch of amino acid residues. The central zinc cation is tetracoordinated as in other LAS enzyme structures, by the usual zinc ligands and a poorly conserved asparagine residue. The location of the asparagine residue downstream of a disordered region in the LytM crystal structure and the analogy to better-characterized lysostaphin-type peptidases suggested that full-length LytM, thought previously to be the active species, may require proteolytic processing for activation. Indeed, we found that the physiologically unrelated peptidase trypsin produced the required cleavage in LytM and strongly activated the enzyme in a pentaglycine digestion assay, a zymography assay with purified *S. aureus* peptidoglycan as the substrate, and in a Remazol dye release assay.[10] We found that $LytM_{185\text{-}316}$, a truncation mutant of LytM that spans residues 185 to 316 and is approximately equivalent to the trypsin-generated fragment, has much higher specific activity than the full-length protein. Together, these results support the idea that LytM, like other lysostaphin-type peptidases, may require a proteolytic maturation step, although it remains to be proven that LytM is processed *in vivo* and the physiologically relevant activating peptidase remains to be identified.

Here, we present a biochemical characterization and three crystal structures of $LytM_{185\text{-}316}$, the first crystal structures of an active form of any lysostaphin-like peptidase. We report the synthesis of a phosphinate substrate analogue, which turned out to be an unexpectedly poor inhibitor. Instead of the phosphinate substrate analogue, we find a tartrate molecule from the buffer in the active site of truncated LytM, which prompted us to test four-carbon, dicarboxylic acids as potential inhibitors, and led to the finding that succinate has some inhibitory activity.

Results

Preparation of native $LytM_{185\text{-}316}$

The cloning, expression and purification of $LytM_{185\text{-}316}$ with an N-terminal histidine tag have been described.[10] However, we were concerned that the tag and the presence of multiple metals after affinity purification on a metal-chelating resin may compromise the analysis of the metal-dependence of $LytM_{185\text{-}316}$ activity. Therefore, we cloned and expressed $LytM_{185\text{-}316}$ without the N-terminal histidine tag. The protein was purified by a series of chromatography steps that were adapted from the previous protocol for the purification of untagged, full-length LytM with minor modifications.

The synthesis of *N*-(2,4-dinitrophenyl)-*N*-tetraglycine-ethylenediamine (Gly4-ethylenediamine-Dnp)

From the previous study it was already known that $LytM_{185\text{-}316}$ cleaves penta- and tetraglycine.[10] To make tetraglycine more easily detectable, we synthesized a variant with (2,4-dinitrophenyl)-ethylenediamine attached to the carboxyl end in amide linkage. The tetraglycine derivative is yellow, can be conveniently quantified by the characteristic absorption of its chromophore at 360 nm (ε_{360} = 17,300 $M^{-1}\,cm^{-1}$) and is more soluble in water than underivatized tetraglycine. The kinetic parameters for Gly4-ethylenediamine-Dnp and $LytM_{185\text{-}316}$ were found to be k_{cat} = 0.003 1/s, K_M = 2.3 mM and k_{cat}/K_M = 1.2 $M^{-1}\,s^{-1}$ under standard conditions, namely 20 mM-Tris–HCl (pH 7.5) (unpublished results).

The synthesis of tetraglycine phosphinic acid analogue H-Gly-Glyψ[P(O)(OH)CH_2]-Gly-Gly-OH

Metallopeptidase substrates can usually be converted to good inhibitors by replacing the scissile amide bond with a phosphinate moiety, which is thought to mimic the transition state. Phosphinate substrate analogues have been shown to be good inhibitors of many types of metallopeptidases,[13] including the VanX aminopeptidase, which is an LAS enzyme with clear similarities to $LytM_{185\text{-}316}$. At the outset of the study, tetraglycine and pentaglycine were known to be $LytM_{185\text{-}316}$ substrates, and it was known that tetraglycine was split into diglycines and pentaglycine into diglycine and triglycine. As the pentaglycine digestion pattern could be the result of two alternative amide bond cleavages, we synthesized a phosphinate analogue of tetraglycine, according to the synthesis procedure outlined in Figure 1(a). The HPLC-purified compound was dissolved in water, neutralized to pH 7.5 and assayed for $LytM_{185\text{-}316}$ inhibition. Surprisingly, the tetraglycine phosphinate turned out to have almost no effect on $LytM_{185\text{-}316}$ activity, with a K_i value above 100 mM (Figure 1(b)). Tetraglycine phosphinate was clearly inferior to commercially available monoglycine hydroxamate (Sigma-Aldrich), for which the K_i was determined to be 0.7 mM (Figure 1(c)).

pH effects on LytM activity

Gly4-ethylenediamine-Dnp was used to assay the activity of $LytM_{185\text{-}316}$ over a wide range of pH values. The activity is optimal at neutral pH values, but extends significantly to both the basic and acidic regions. The enzyme has residual activity at best below pH 4.5 and above pH 9.5 (Figure 2).

Effects of divalent metal ions on LytM activity

The metal ion in full-length LytM is known to be zinc, because the structure was solved, in part, by MAD phasing on the zinc edge.[10] However, because the enzyme was recombinantly overproduced in a heterologous host, the metal content may not be representative. To assess the effect of different divalent metal ions on the enzyme activity, $LytM_{185\text{-}316}$ was treated with 10 mM EDTA to chelate out the original metal ions, and then dialyzed extensively against buffer A to remove excess EDTA. The TLC-assay with Gly4-ethylenediamine-Dnp indicated that the activity could be restored by Zn^{2+}, Co^{2+}, Mn^{2+} and partially also Ni^{2+}, but not by Cu^{2+}, Ca^{2+} or Mg^{2+} (Figure 3(a)).

To make the results quantitative, the cleavage of Gly4-ethylenediamine-Dnp was monitored by HLPC. Digests were done with 4 mM Gly4-ethylenediamine-Dnp, the concentration which is

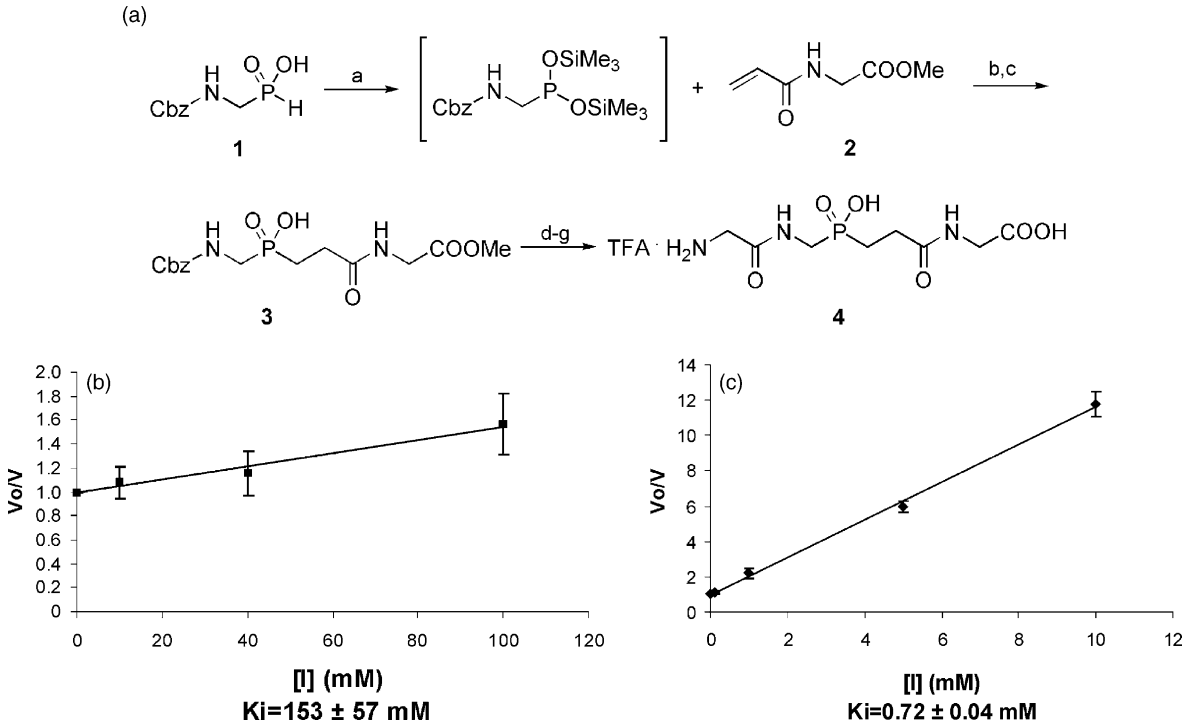

Figure 1. (a) Outline of the synthesis of the phosphinate analogue of tetraglycine. Reagents and conditions: (a) hexamethyldisilazane, 90–100 °C, 2 h; (b) hexamethyldisilazane, 80–90 °C, 3 h; (c) MeOH, yield 85% starting from **1**; (d) 33% HBr/AcOH, room temperature, 2 h; (e) Cbz-Gly-OH, isobutyl chloroformate, *N*-methylmorpholine, anhydrous tetrahydrofuran (THF), 0 °C → room temperature, overnight; (f) bromotrimethylsilane, anhydrous CH_2Cl_2, 3d, room temperature, (g) water, then conc. HCl, then HPLC, yield 15% starting from **3**. (b) Effect of the tetraglycine phosphinate analogue on $LytM_{185\text{-}316}$ activity. (c) Effect of glycine hydroxamate on $LytM_{185\text{-}316}$ activity. The assays in (b) and (c) were done with 10 μM enzyme and 0.5 mM Gly4-ethylenediamine-Dnp, which is below the K_m for this substrate, so that apparent and actual inhibition constants are related by a correction factor close to 1.

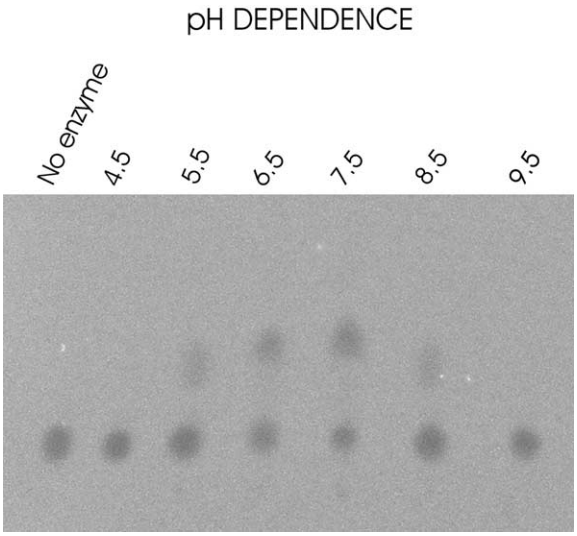

Figure 2. $LytM_{185\text{-}316}$ activity in TLC assay as a function of the pH. The assay was done with 100 μM enzyme and 4 mM Gly4-ethylenediamine-Dnp, which is above the K_m for this substrate at neutral pH. The lower spots correspond to the Gly4-ethylenediamine-Dnp substrate, the upper to the Gly2-ethylenediamine-Dnp product.

above the K_m (2.3 mM) for this compound. Substrate turnover was strongly reduced after the metal-depletion step, and could be quantitatively restored by the addition of a twofold molar excess of Zn^{2+} over the enzyme. The activity was partially recovered with Co^{2+}(63%) and Mn^{2+}(66%), but not with Cu^{2+}(22%) (Figure 3(b)). The metals in a twofold molar excess over the enzyme had almost no detectable effect when they were added to preparations of $LytM_{185\text{-}316}$ that had not been subjected to the metal-depletion step (Figure 3(c)).

$LytM_{185\text{-}316}$ crystallization

Three different crystal forms of $LytM_{185\text{-}316}$ could be grown. The first crystals were trigonal, belonged to space group *P*3(2)21 and diffracted to 1.83 Å at BW6, DESY, but appeared at pH 4.5, which is too acidic to support enzyme activity. We therefore searched for new crystallization conditions in the pH-range 5.5–8.5, where the enzyme is active. At pH 6.5, orthorhombic crystals could be grown. They belonged to space group *P*2(1)2(1)2(1) and diffracted to 1.55 Å at BW6, DESY. When we screened for crystallization conditions of $LytM_{185\text{-}316}$ in the presence of 20 mM tetraglycine phosphinate, a tetragonal crystal form, space group *P*4(1), was found. These crystals diffracted to 1.55 Å on an in-house, rotating anode X-ray system, but instead of the phosphinate analogue, they contained a tartrate molecule from the reservoir buffer bound in the active site.

Comparison of $LytM_{185\text{-}316}$ structures

Each of the three crystal forms contained two monomers in the asymmetric unit, so that altogether six models of $LytM_{185\text{-}316}$ were available for comparison with the full-length enzyme. Superposition of the C^{α} traces showed that the models are

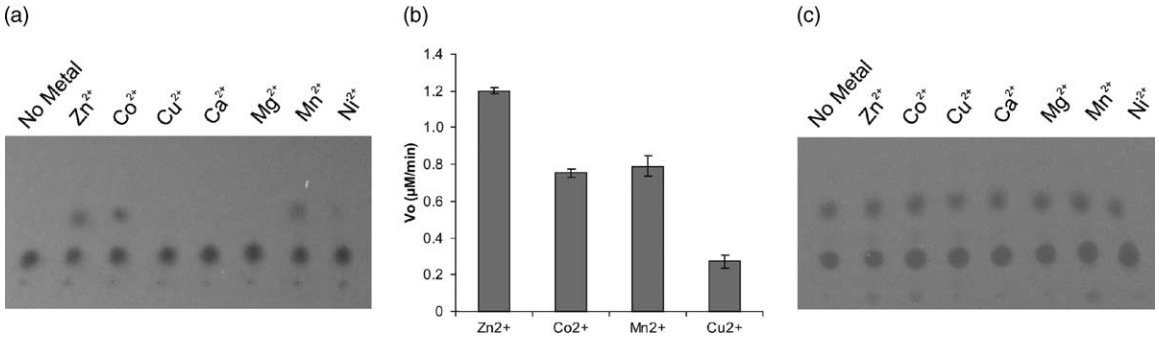

Figure 3. Effects of divalent metal ions on $LytM_{185\text{-}316}$ activity. (a) Metal reactivation of Zn^{2+}-depleted $LytM_{185\text{-}316}$ was tested in a TLC-based activity assay after 30 min preincubation with the indicated metal ions at 37 °C. Spots corresponding to the substrate (lower) and the product (upper) were visualized by exposure to UV light. (b) HPLC-based assay demonstrating the quantitative measurement of Zn^{2+}-depleted $LytM_{185\text{-}316}$ reactivation by selected divalent cations. The initial velocity was determined for an apo-$LytM_{185\text{-}316}$ as control, and for Zn^{2+}-depleted $LytM_{185\text{-}316}$ preincubated with appropriate metal ions: Zn^{2+}, Co^{2+}, Mn^{2+}, Cu^{2+}. (c) The influence of different metal ions on Zn^{2+}-containing $LytM_{185\text{-}316}$ was tested by the TLC-based activity assay.

all similar, particularly models for molecules in the same asymmetric unit. A superposition of all six crystal forms of $LytM_{185-316}$ with the latent LytM shows that no major conformational changes are induced by the removal of the inhibitory N-terminal region (Figure 4(a)). The superposition of all six $LytM_{185-316}$ models with the equivalent part of the full-length enzyme confirms that the $LytM_{185-316}$ structure is largely rigid, except in four loop regions that are built from residues 200–212, 237–242, 281–290 and 299–305 (Figure 4(a) and (b)). A comparison of the all-atom models revealed distortions in the active sites of the $LytM_{185-316}$ molecules in the asymmetric unit of the trigonal crystals (see below).

Overall $LytM_{185-316}$ structures

The most striking feature of the $LytM_{185-316}$ structures is the extended, long and narrow groove with the active site metal ion at the bottom. The floor of the groove is formed by the central β-sheet that is one of the hallmarks of LAS enzymes. The groove is lined on the sides by the four loop regions that are the regions of highest variability among the altogether six $LytM_{185-316}$ models and the full-length LytM model. In the orthorhombic and tetragonal crystal forms, the groove is largely continuous (Figure 4(c)). In the trigonal crystal form, the loop region 281–290 is drastically rearranged in both monomers in the asymmetric unit. The change brings asparagine 286 so close to tyrosine 204 OH that the central groove is essentially divided into two regions (Figure 4(a) and (d)).

Substrate binding

The failure of the phosphinate tetraglycine analogue to inhibit $LytM_{185-316}$ appreciably and our inability to obtain cocrystals with this putative substrate analogue forced us to look for indirect evidence that the extended, central groove in the $LytM_{185-316}$ structure is indeed the substrate-binding cleft. The presence of three consecutive glycines residues, Gly 206 to Gly 208, in one of the most exposed loops of the LytM structure, turned out to be very helpful. In the P4(1) crystal structure, the loop of monomer A inserts into the groove of monomer B, where it comes into the immediate vicinity of the active site Zn^{2+} (Figure 4(c) and 5(a)). In the *P*3(2)21 crystal structure, monomer A packs against a crystallographic symmetry mate, so that the loops

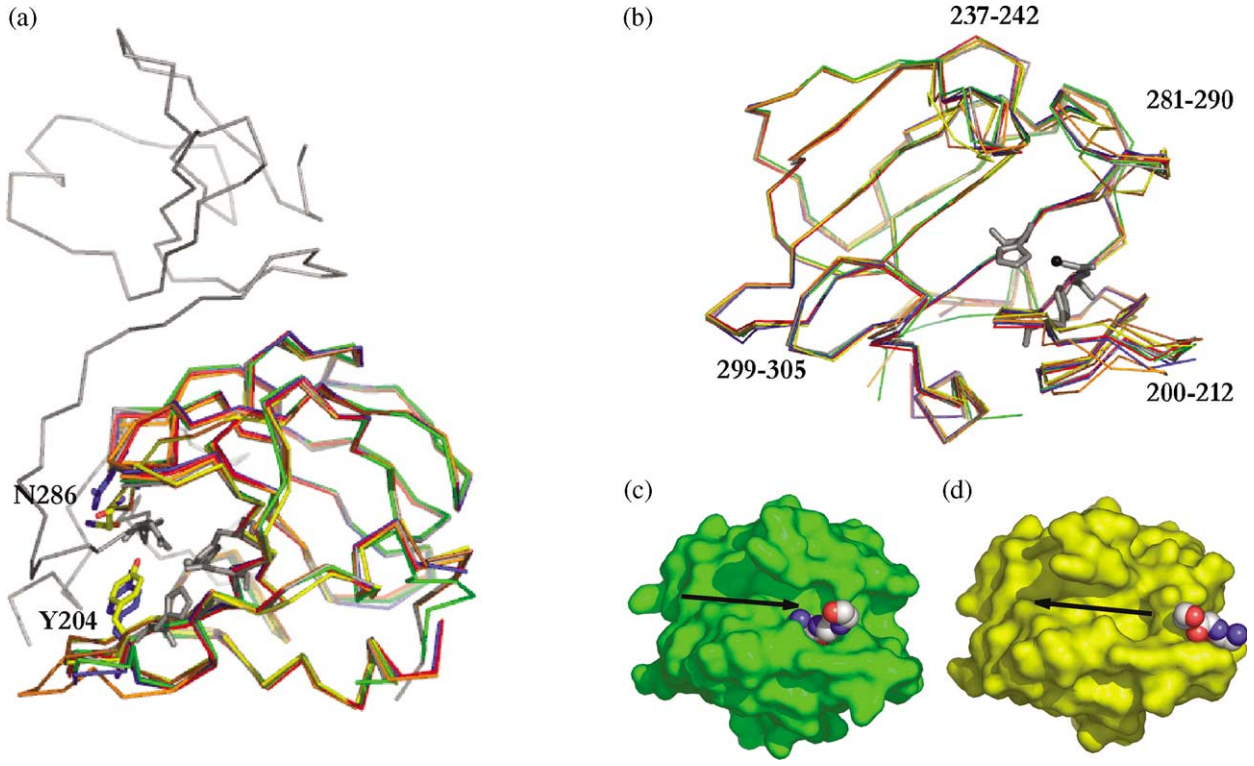

Figure 4. Superposition of the six models of $LytM_{185-316}$ with full-length LytM (PDB accession code 1QWY). The full-length LytM is shown in grey, the models for the *P*3(2)21 form are in yellow (molecule A) and brown (molecule B), the models for the $P2_12_12_1$ form are in blue (molecule A) and red (molecule B), and the models for the $P4_1$ form are in orange (molecule A) and green (molecule B). (a) Side view to illustrate the groove, and (b) top view to show the flexibility of the groove walls. (c) Molecule B of the $P4_1$ form in surface representation. The triglycine of a loop of the neighbouring molecule A is shown in CPK representation. (d) Molecule A of the $P3_221$ form in surface representation. The triglycine of a loop of a crystallographic symmetry mate of molecule A is shown in CPK representation. For (d), one of the two conformations of the loop and the compatible receptor conformation were chosen. The arrows in (c) and (d) indicate the direction of the polypeptide chain in the triglycine loop.

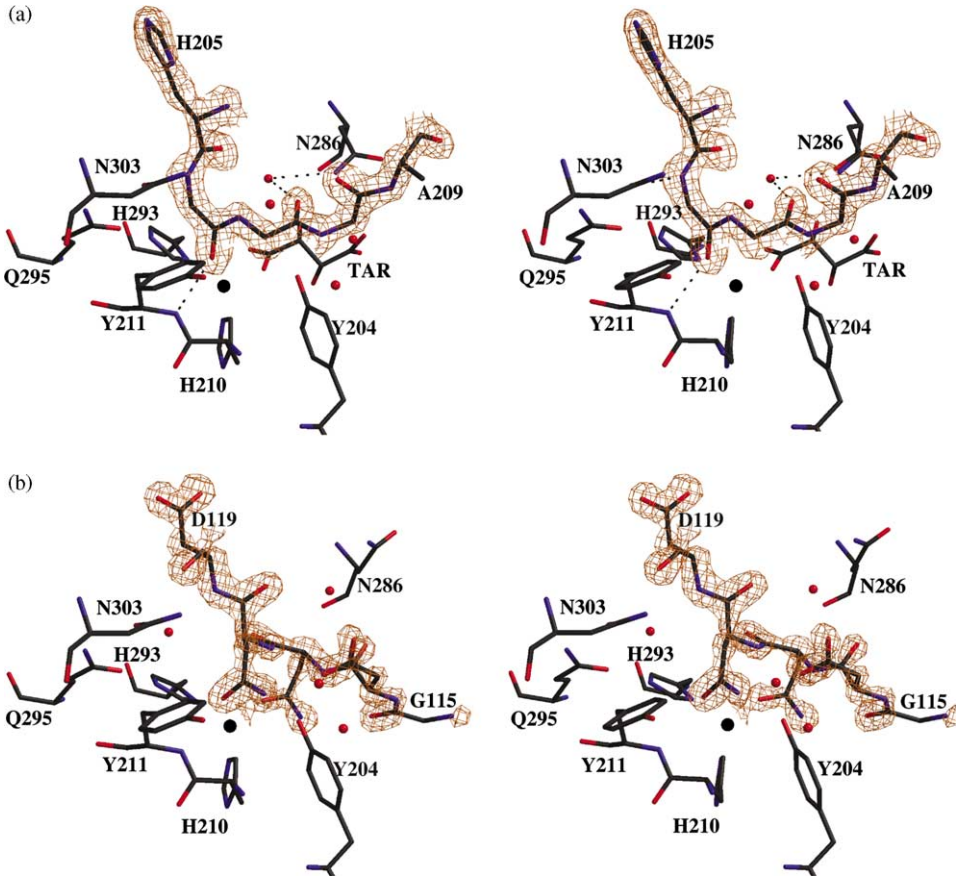

Figure 5. Binding mode comparison. (a) Stereo diagram of the interaction of the glycine-rich loop of monomer B (shown with omit map density, contoured at 1.5 σ) with the active site region of monomer A in the $P4_1$ crystal form. Residues of monomer B and water molecules that come closer than 3.5 Å to the three glycine residues are presented in ball-and-stick representation in standard colour-coding and without density. The black ball represents Zn^{2+}. For orientation, the tartrate molecule in the active site of this crystal form has been included in the drawing. Hydrogen bonds to or from the three loop glycine residues are indicated by broken lines. All interactions in (a) result from the packing of the $P4_1$ crystal form and are not present in the other crystal forms. (b) Stereo diagram of the interaction of the N-terminal part of full-length LytM (shown with omit map density, contoured at 2.0 σ) with the active site region of the latent enzyme. For comparison, the same residues of the active LytM region as in (a) are drawn, irrespective of whether they interact with the N-terminal part.

from the two molecules are placed in the central grooves of the other molecule (Figure 4(d)). It appears that two conformations are present, which are mutually exclusive in adjacent *P*3(2)21 unit cells. A detailed discussion of the resulting crystallographic complications is presented in the Supplementary Data. Despite the complication from multiple conformations in the *P*3(2)21 crystal form, it is clear that the loop glycine residues fill different parts of the $LytM_{185\text{-}316}$ groove in the *P*4(1) and *P*3(2)21 crystal forms. A comparison with the previous structure of latent LytM[10] further shows that the binding modes are different from the binding mode of the occluding N-terminal region of the full-length enzyme (Figure 5).

Active sites

The geometry of the metal-chelating residues, histidine 210, aspartate 214 and histidine 293 is strictly conserved in all three crystal forms and identical with the arrangement in full-length LytM.

In the trigonal and orthorhombic crystal forms, the metal is tetrahedrally coordinated. As the truncated $LytM_{185\text{-}316}$ proved to be catalytically active, we expected to find a water molecule as the fourth Zn^{2+} ligand in the active site, in place of asparagine 110 of full-length LytM. Instead, we found that the fourth ligand in both crystal forms had clearly tetrahedral shape. The trigonal crystal form was grown with 2 M ammonium dihydrogen phosphate in the crystallization buffer; therefore, the extra ligand was interpreted as a phosphate mono-anion. The phosphate molecule is fixed in space by multiple hydrogen bonds: the oxygen atom O4, which coordinates the Zn^{2+}, accepts a hydrogen bond from the OH of tyrosine 204 and the oxygen O3 from two active site histidine residues: N^{δ} of histidine 260 and N^{ε} of histidine 291. The protonated oxygen atom O1 donates a hydrogen bond to O^{δ} of asparagine 286, protruding into the active site cleft in this crystal form, and accepts a hydrogen bond from the backbone nitrogen atom of asparagine 286 (Figure 6(a)).

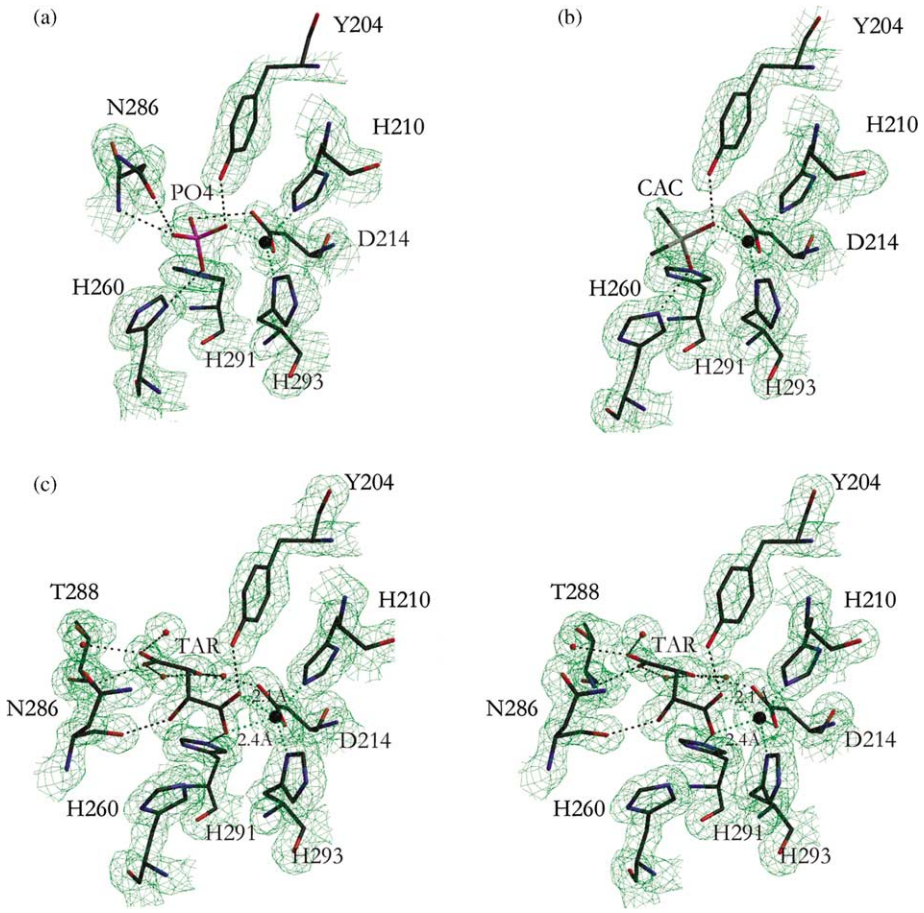

Figure 6. Ball-and-stick representation of the selected residues of the active site of $LytM_{185\text{-}316}$. The electron density covering these residues is shown. The densities are $2F_o - F_c$ omit maps, calculated omitting all residues and ligands shown in the Figure, contoured at 1σ. The Zn^{2+} is shown as a black ball, and water molecules are shown as red balls. All Zn^{2+}-coordinating interactions are represented by green, dotted lines. Hydrogen bonds are indicated by black, dotted lines. (a) The trigonal form with the monohydrogen phosphate anion (PO_4). (b) The orthorhombic form with the cacodylate anion (CAC). (c) The tetragonal form with the tartrate molecule (TAR) interacting with Zn^{2+} and other active site residues shown in stereo.

The orthorhombic crystal form was grown with 0.2 M sulphate and 0.1 M cacodylate (dimethyl arsenate) in the crystallization buffer. Although the concentration of sulphate is double the concentration of cacodylate, the extra density near the zinc ion was interpreted as a cacodylate ion, for several reasons. (a) HSO_4^- and SO_4^{2-} are extremely weak bases, in contrast to cacodylate, which has a pK_b near neutral and is therefore expected to be the better Zn^{2+} ligand. (b) The absence of water molecules near the methyl groups of cacodylate makes sense, whereas the lack of water molecules near two oxygen atoms of a sulphate ion would be counterintuitive. (c) The bond lengths are more consistent with the cacodylate interpretation. (d) The refined *B*-factors are more even if the central atom is taken to be arsenic (33 electrons) rather than sulphur (16 electrons). (e) There is a clear peak for the central atom in the dispersive difference Fourier map, ($F_{1.54\ Å} - F_{1.05\ Å}$) calculated with the phases of the final model omitting the Zn^{2+} and the ligand coordinating it, as would be expected for arsenic ($\Delta f'$, 1.54 Å *versus* 1.05 Å ≈ 2), but not for sulphur ($\Delta f'$ 1.54 Å *versus* 1.05 Å ≈ 0.1)[14] (Figure 6(b)).

In the tetragonal crystal form, tartrate molecules from the buffer are captured in the active sites. The density is very clear in one monomer (designated B in the deposited PDB file) and much weaker in the other monomer (designated A in the deposited file), where the occupancy of the ligand is only partial. The excellent electron density for the tartrate molecule in monomer B allowed us to define the stereochemistry as L(+). Among all possible stereoisomers, this assignment yielded the lowest *R*-factor after ligand refinement and was consistent with the stereoisomer in the buffer. The tartrate molecules are in contact with the zinc ions *via* one of their carboxylate groups. In the well-defined monomer B, the distances from the tartrate oxygen atoms to the metal ion are 2.1 Å and 2.4 Å, and clearly different. The values are typical for first coordination sphere ligands and for weakly interacting ligands, respectively.[15] We note that similarly

"asymmetric" interactions between a carboxylate group and a zinc ion have been described before in other metallopeptidases, such as matrilysin or thermolysin.[16] As the amino acid Zn^{2+} ligands are at their usual distances from the Zn^{2+}, the metal coordination can be described as semi-pentacoordinate (Figure 6(c)).

The L(+)-tartrate molecule in the active site interacts with $LytM_{185\text{-}316}$ not only *via* the metal ion. The oxygen atoms that coordinate the Zn^{2+} are within hydrogen bonding distance to tyrosine 204 OH and histidine 291 N^{ε}. The two tartrate hydroxyl groups donate hydrogen bonds to aspartate 214 O^{δ} and asparagine 286 O, and one of the oxygen atoms of the carboxylate group that is not involved in metal chelation accepts a hydrogen bond from threonine 288 N. The other oxygen atom of this carboxylate group is in contact with the solvent.

Effects of dicarboxylic acids on $LytM_{185\text{-}316}$ activity

The fit of L(+)-tartrate into the $LytM_{185\text{-}316}$ prompted us to check the effects of L(+)-tartrate, meso-tartrate, D(−)-tartrate, L(−)-malate, D(+)-malate, and succinate on $LytM_{185\text{-}316}$ activity. Only succinate, $K_i = 3.9$ mM and L(−)-malate, $K_i = 15$ mM, inhibited $LytM_{185\text{-}316}$ appreciably. For all other compounds, including L(+)-tartrate, the K_i is higher than 200 mM and is difficult to determine (data not shown).

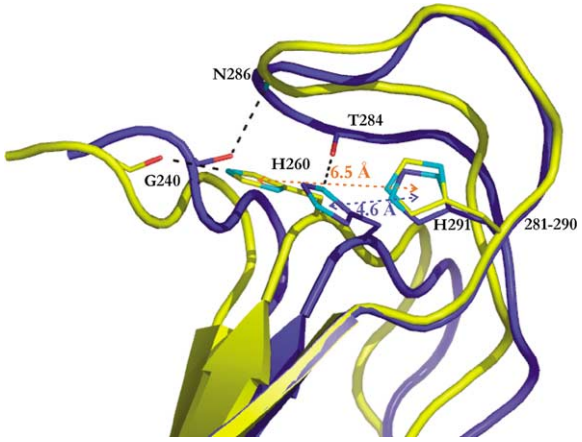

Figure 7. Distortion of the active site in the $P3_221$ form. The active site Zn^{2+}-coordinating residues of molecules A of the $P3_221$ form (yellow) and of the $P2_12_12_1$ form (blue) were superimposed. The Figure shows selected fragments of the $LytM_{185\text{-}316}$ structure in the proximity of H260 and H291, and the loop 281–290, located above them. The hydrogen bonds that have changed upon the rearrangement are shown as black, broken lines. The distances between the centroids of H260 and H291 are indicated by broken-line-arrows. Note that H260 in the trigonal form is flipped around the C^{β}–C^{γ} bond in comparison with H260 in the orthorhombic form, which is representative of all crystal structures obtained at pH around neutral.

Discussion

Do the $LytM_{185\text{-}316}$ structures explain the pH activity profile?

The orthorhombic and tetragonal crystals were grown at pH 6.5, where the enzyme is active. In contrast, the trigonal crystals were obtained at pH 4.5, which does not support enzyme activity. As the Zn^{2+} in the active site is supported by robust electron density also in this crystal form, a loss of the metal ion cannot account for the lack of activity. We therefore looked for features that distinguished the $LytM_{185\text{-}316}$ models for the acidic crystal form from all other models and found distortions in the active site and loop rearrangements.

The most striking difference involves histidine 260 and 291. These two residues are not involved in metal chelation, but are conserved in nearly all LAS enzymes and are therefore likely to have a catalytic role. In the acidic crystal form, the distance between the imidazole rings of these two histidine residues is significantly larger than in all other LytM and $LytM_{185\text{-}316}$ structures, probably because both imidazole rings are protonated and repel each other. Moreover, the imidazole ring of histidine 260 is flipped around the C^{β}–C^{γ} bond, which alters the hydrogen bonding pattern and may, at least in part, explain the movement of the loop 281–290, which is located immediately above histidine 260 and 291. The rearrangement in the trigonal crystal form brings asparagine 286 so close to tyrosine 204 OH that the central groove is divided, which may explain the experimentally observed lack of activity at acidic pH (Figures 2 and 7).

How does $LytM_{185\text{-}316}$ bind substrate?

As the phosphinate tetraglycine analogue did not inhibit $LytM_{185\text{-}316}$ appreciably and was not found in crystals that were grown in its presence, the detailed substrate-binding mode remains unknown. Nevertheless, crystal packing effects, which place three consecutive glycine residues from an exposed loop in the central groove of neighbouring molecules, support the idea that the groove is indeed the substrate-binding cleft. However, it is also clear that the detailed binding mode of the loop fragments cannot be fully substrate-like. First, in both cases the loop fragments are inserted on one side of the active site cleft only, and do not run across the active site. As a result, there is continuous electron density for the loops, which confirms that the loops do not behave as substrates and are not cleaved. Second, the polypeptide chains of the glycine fragments in the $LytM_{185\text{-}316}$ active site cleft run in opposite directions, so that, at best, one of the glycine-fragments can be a good substrate mimic. A comparison with a VanX-substrate complex[4] does not support either binding mode, but may not be relevant, because it is unclear whether lysostaphin-like enzymes and VanX-like enzymes are homologous or analogous.

Inhibitor sensitivity

Gly4-ethylenediamine-Dnp has moderate, millimolar affinity for $LytM_{185-316}$. We expected that the transition state analogue H-Gly-Glyψ[P(O)(OH)CH_2]-Gly-Gly-OH should bind tighter than a substrate, and therefore hoped for a submillimolar affinity of the substrate analogue. Surprisingly, it turned out that the compound bound to $LytM_{185-316}$ hardly at all. We suspected that $LytM_{185-316}$ could attack amide bonds in H-Gly-Glyψ[P(O)(OH)CH_2]-Gly-Gly-OH and might destroy the compound, but mass spectra of the compound recorded before and after incubation with the enzyme excluded this possibility. The experimentally measured mass of the compound in M[-]-mode, 280.2 Da, agreed perfectly well with the calculated mass, 280.19 Da.

In contrast to phosphinate analogues of substrates, peptide hydroxamates are unsuitable as mechanistic probes, but they are expected to be better inhibitors, because hydroxamates are stronger Zn^{2+}-coordinating groups than phosphinates.[17] This general expectation turned out to be true for our special case, as even monoglycine hydroxamate showed at least some inhibitory activity against $LytM_{185-316}$.

The surprise finding of L(+)-tartrate from the buffer in the active site of the tetragonal crystals suggested that this small compound could have appreciable inhibitory activity against $LytM_{185-316}$. Calculations with the ligand scoring program Xscore[18] predicted an affinity below 100 μM for the $LytM_{185-316}$–L(+)-tartrate complex. Moreover, because essentially all functional groups are involved in hydrogen bonding interactions, one would expect that other three of four carbon dicarboxylic acids should have lower affinity for the enzyme than L(+)-tartrate. The biochemical results prove both predictions wrong, the first one spectacularly so: the affinity between $LytM_{185-316}$ and L(+)-tartrate in solution is at least a 1000-fold lower than predicted (data not shown), and in fact so low that L(+)-tartrate, which is present in the crystallization drop at a concentration below 200 mM, should not even be fully bound. This is indeed the case in subunit A, where the density for the L(+)-tartrate molecule is poor. It is known from the superpositions that in subunit B, the molecule takes an unusual conformation, probably induced by both the presence of the L(+)-tartrate and by the insertion of the loop with the three glycine residues of subunit A. Moreover, most of the residues in contact with the L(+)-tartrate belong to the most flexible regions of the structure. Therefore, we assume that the L(+)-tartrate-binding conformation can only be taken at the cost of a large free energy penalty, and that neglect of this penalty in the Xscore calculations accounts for the discrepancy with the biochemical data. If correct, this explanation also implies that the modest inhibitory activity of succinate is due to a different binding mode. Unfortunately, this hypothesis could not be verified, because $LytM_{185-316}$ could so far not be crystallized in the presence of succinic acid.

Materials and Methods

Protein cloning, overexpression and purification

The cloning of $LytM_{185-316}$ with a non-cleavable histidine tag was reported before.[10] For this study, the protein without the N-terminal histidine tag was required. Therefore, a fragment of the *lytM* gene, corresponding to the catalytic C-terminal domain, was amplified from genomic DNA of *S. aureus* NCTC8325. The PCR product was cloned into the pET15b expression vector (Novagen) after cleavage with the restriction enzymes NcoI and XhoI, transformed into *E. coli* strain BL21 (DE3), and grown in 37 °C to $A_{600}=0.8$. Overexpression of the protein was induced with 1 mM IPTG, and the cells were harvested after a 4 h incubation period in 25 °C. Cells were disrupted by sonication, the supernatant clarified by ultracentrifugation, and the protein purified essentially according to the protocol that was established for the purification of the untagged, full-length form,[10] except that the gel-filtration step was performed in 10 mM Tris (pH 7.5), 200 mM NaCl buffer. In this buffer, the protein was stable and could be stored for two months in the cold room without the loss of activity.

Zn^{2+} removal and re-uptake

In order to obtain Zn^{2+}-depleted $LytM_{185-316}$, the purified enzyme was incubated in the presence of 10 mM EDTA for 1 h at room temperature and subsequently dialyzed extensively against buffer A (10 mM Tris (pH 7.5), 50 mM NaCl). Finally, the apo-$LytM_{185-316}$ was concentrated and subjected to gel-filtration on Sephacryl S-200 HR (Amersham Pharmacia). Metal re-uptake was accomplished by adding 100 μM metal salts to 50 μM apo-$LytM_{185-316}$, and by incubating for 60 min at 37 °C in buffer A.

The chemical synthesis of H-Gly-Gly-Gly-Gly-$NHCH_2$-CH_2NH-Dnp trifluoroacetate

Boc-Gly-Gly-OH (0.46 g, 2 mmol) was activated by means of isobutyl chloroformate (0.27 ml, 2.1 mmol) and *N*-methylmorpholine (0.25 ml, 2.2 mmol) in anhydrous tetrahydrofuran (THF) (10 ml) using the mixed anhydride procedure. After 1 h of stirring *N*-(2,4-dinitrophenyl) ethylenediamine[19] was added. The pH of the suspension was adjusted to basic with addition of *N*-methylmorpholine. After stirring overnight the solvent was removed *in vacuo*. The residue was taken up with ethyl acetate (30 ml) and water (10 ml) and washed consecutively with 5% $NaHCO_3$ (20 ml), 5% citric acid (2×20 ml), 5% $NaHCO_3$ (20 ml) and brine (20 ml). The organic layer was dried over anhydrous Na_2SO_4 and evaporated to dryness yielding 0.33 g (75%) of crude bright yellow Boc-Gly-Gly-$NHCH_2CH_2NH$-Dnp of satisfactory purity. The obtained dipeptide analogue was treated with trifluoroacetic acid (TFA) (5 ml). After 30 min of stirring the acid was removed *in vacuo*. A suspension of Boc-Gly-Gly-OH (0.35 g, 1.5 mmol) activated in the standard way (see above) was added to this residue. The subsequent coupling reaction was performed and worked up in the same manner as the preceding one. Finally protected teterapeptide analogue was separated upon addition of diethyl ether (20 ml) to the crude product yielding 0.36 g (65%) of yellow solid. A 50 mg sample was used for Boc deprotection (TFA, 2 ml, 30 min) and for HPLC purification (performed on Varian ProStar apparatus with ProStar 325 UV/Vis detector using Dynamax 250×21.4

Microsorb 300-10 C18 column; A and B mobile phase refers to water and acetonitrile respectively, both containing 0.1% TFA) giving pure yellow H-Gly-Gly-Gly-Gly-$NHCH_2CH_2NH$-Dnp trifluoroacetate (Gly4-ethylenediamine-Dnp) after lyophilization. HPLC gradient: $t=0$ min (10% B), $t=18$ min (34% B). R_t 17.4 min. ^1H NMR (300.13 MHz, ^2H_2O): δ 3.61, 3.72 (m each, 2H and 2H, NCH_2CH_2N), 3.89, 3.96, 4.00, 4.10 (s each, 2H, 2H, 2H and 2H, $4\times CH_2$), 7.17 (d, $J=9.5$ Hz, 1H, H_{ar}), 8.33 (d, $J=9.5$ Hz, 1H, H_{ar}), 9.12 (s, 1H, H_{ar}).

TLC-based activity assay

$LytM_{185\text{-}316}$ (100 μM) was incubated with Gly4-ethylenediamine-Dnp (4 mM) for 3 h at 37 °C in 10 mM-Tris–HCl (pH 7.5) buffer, unless the pH-dependence was tested. In this case, different buffers were used, namely 20 mM sodium citrate (pH 4.5), 20 mM Mes (2-(*N*-morpholino)-ethanesulfonic acid) (pH 5.5 and 6.5), 20 mM Tris (pH 7.5 and 8.5) and 20 mM PBC (propionate, cacodylate, bis-Tris propane) (pH 9.5). The reaction was stopped by the addition of trace amounts of 1% TFA and the 2 μl samples were applied onto a TLC plate covered by silica gel. Subsequently, plates were dried and developed in the mobile phase containing *n*-butanol/acetic acid/water (4:1:1, by vol.). Due to the presence of the Dnp group in the substrate, the visualization of the spots could be done *via* the exposure to UV light.

HPLC-based activity assay

The enzyme (10 μM) was preincubated with appropriate inhibitor or the metal ion, depending on the assay, in 20 mM Tris–HCl (pH 7.5) buffer for 30 min at 37 °C. The reaction was initiated by the addition of 0.5 mM Gly4-ethylenediamine-DnpDNP in the inhibition assay or 4 mM Gly4-ethylenediamine-Dnp in the case of metal reactivation assay, and incubated at 37 °C. The samples were collected after 0, 30 min, 60 min and 90 min. The reaction was stopped by mixing the reaction solution 1:1 with 0.1% TFA. The sample (20 μl) with 0.1% TFA was subjected to HPLC separation, which was performed on a NUCLEOSIL 100-5 C18 column (3 mm ID, 150 mm) (Marchery Nagel) equilibrated with 0.1% TFA in MilliQ water. A linear gradient was generated from 0% to 50% acetonitrile in 0.1% TFA at 30 min at a flow-rate of 0.5 ml/min, and absorption of the eluate was measured at 357 nm, the wavelength that corresponds to peak maximum for both the substrate (Gly4-ethylenediamine-Dnp, $R_t=17.2$ min and the product (Gly2-ethylenediamine-Dnp, $R_t=18.1$ min). The amount of the product was determined from the peak area, by use of a standard curve generated with purified Gly4-ethylenediamine-Dnp. The error estimates based on standard deviation were derived from repetitions of three independent incubations.

In all assays in which the inhibitory effect of different compounds on $LytM_{185\text{-}316}$ activity was tested, initial velocity in the absence of inhibitor *versus* the initial velocity in the presence of the inhibitor (V_0/V) was measured. This ratio is expected to depend on the apparent K_i^* ($V_0/V=1+[I]/K_i^*$), where [I] is the inhibitor concentration. Subsequently, the apparent K_i^* were corrected according to the equation $K_i=K_i^*/(1+[S]/K_M)$.

The chemical synthesis of tetraglycine phosphinic acid analogue (H-Gly-Glyψ[P(O)(OH)CH_2]-Gly-Gly-OH, 4)

The first step of the procedure involved synthesis of *N*-benzyloxycarbonylaminomethanephosphinic **1**. The phosphinic analogue of glycine was obtained by treatment of 1,3,5-tris(*N*-diphenylmethyl)hexahydro-*s*-triazine (19.5 g, 0.033 mol) with ~1 M solution of methyl ester of hypophosphorus acid prepared from anhydrous H_3PO_2[20] (6.6 g 0.1 mol), methyl orthoformate (48 ml), anhydrous toluene (24 ml) and THF (24 ml).[21,22] Then, the adduct was hydrolysed in acidic conditions and the obtained amino acid was *N*-protected with benzyl chloroformate in basic conditions as described in the literature.[23,24] The overall yield of the procedure was 45%. Mp, 90–91 °C (colourless crystals recrystallized from ethyl acetate/toluene), lit. mp, 95–96 °C.[24] ^{31}P NMR (121.50 MHz, $^2H_2O/NaO^2H$): δ 23.00. ^1H NMR (300.13 MHz): δ 3.18 (dd, $J_1=9.6$ Hz, $J_2=1.6$ Hz, 2H, NCH_2P), 5.04 (s, 2H, CH_2O), 6.88 (d, $J=522.8$ Hz, 1H, P*H*), 7.35 (m, 5H, C_6H_5).

The second component, *N*-acryloylglycinate **2** was obtained using the mixed anhydride procedure. This accomplished the activation of acrylic acid (1.44 g, 0.02 mol) to the corresponding anhydride by means of isobutyl chloroformate (2.72 ml, 0.021 mol) in the presence of *N*-methylmorpholine (2.33 ml, 0.021 mol) in anhydrous THF (20 ml) at 0 °C. After 1 h of stirring, another portion of *N*-methylmorpholine (2.33 ml, 0.021 mol) was added followed by methyl glycinate hydrochloride (2.51 g, 0.02 mol). Stirring was continued overnight, the separated ammonium salt was filtered off and the solvent was removed *in vacuo*. The residue was purified by column chromatography (silica gel 60, 70–230 mesh) using ethyl acetate as the eluent. The final product was obtained as colourless oil slowly crystallizing in the fridge. Yield, 70%. ^1H NMR (300.13 MHz): δ 3.74 (s, 3H, CH_3), 4.11 (d, $J=5.3$ Hz, 2H, CH_2), 5.68 (dd, $J_1=10.0$ Hz, $J_2=1.7$ Hz, 1H, $=CH$), 6.25 (ABX system, $J_{AB}=17.0$, $J_{AX}=10.0$ Hz, $J_{BX}=1.7$ Hz, 1H, $=CH_2$), 6.41 (bs, 1H, N*H*).

The phosphinic pseudotripeptide analogue Cbz-Glyψ[P(O)(OH)CH_2]-Gly-Gly-OMe **3** was obtained by Michael addition of the acrylate to the aminophosphinic substrate preactivated into the form of its silyl ester as reported earlier[25,26] with minor modifications. To convert compound **1** (1.15 g, 5 mmol) into the trivalent ester it was heated with hexamethyldisilazane (5.3 ml, 25 mmol) at 90–100 °C for 2 h under nitrogen. Then, the reaction mixture was cooled to 40 °C and methyl *N*-acryloylglycinate **2** (0.86 g, 6 mmol) was added. The temperature was maintained at 80–90 °C for an additional 3 h while dense oil precipitated. After cooling to 40 °C, methanol (25 ml) was added dropwise and the mixture was refluxed until its homogenisation. Then, the volatile components were removed under reduced pressure, the residue was redissolved in MeOH (25 ml) and acidified with few drops of 4 M HCl/dioxane. The precipitated inorganic salt was filtered off. The filtrate solution was treated with diethyl ether (200–250 ml) to yield a white amorphous solid of the tripeptide **3** of satisfactory purity. Yield, 85%. ^{31}P NMR (121.50 MHz, CD_3OD): δ 47.92. ^1H NMR (300.13 MHz): δ 2.08 (m, 2H, PCH_2), 2.60 (m, 2H, PCH_2CH_2), 3.56 (d, $J=8.4$ Hz, 2H, NCH_2P), 3.75 (s, 3H, CH_3), 3.97 (s, 2H, CH_2), 5.14 (s, 2H, CH_2O), 7.35 (m, 5H, C_6H_5).

The phosphinic pseudotetrapeptide Cbz-Gly-Glyψ[P(O)(OH)CH_2]-Gly-Gly-OH was synthesized by elongation of the N terminus of the appropriate tripeptide with N-benzyloxycarbonylglycine as described for shorter analogues.[27] The benzyloxycarbonyl group was removed from compound **3** (0.37 g, 1 mmol) by action of 33% HBr in AcOH (3 ml, 2 h). After evaporation to dryness the residue was additionally washed with diethyl ether (3×20 ml) to remove benzyl bromide. Solution of

Table 1. Data collection and refinement statistics

A. *Data collection statistics*			
Space group	$P3_221$	$P2_12_12_1$	$P4_1$
Unit cell parameters			
a, *b*, *c* (Å)	100.4, 100.4, 103.0	32.1, 78.3, 102.1	66.0, 66.0, 63.0
α, β, γ (deg.)	90, 90, 120	90, 90, 90	90, 90, 90
Independent reflections	51,861	39,977	38,546
Resolution (Å)	1.83	1.5	1.55
Completeness (%)	97.6	99.9	96.3
R_{sym} (last shell) (%)	6.3 (24.4)	6.8 (25.6)	3.7 (15.2)
I/σ (last shell)	27.6 (4.7)	6.4 (2.7)	25.8 (10.0)
B. *Refinement statistics*			
R-factor (%)	18.1	18.0	17.2
R_{free} (%)	19.3	22.2	20.1
rmsd bond lengths (Å)	0.017	0.017	0.013
rmsd bond angles (deg.)	1.7	1.7	1.5
B (isotropic) from Wilson (Å^2)	31.9	13.8	15.0
Ramachandran plot			
Core (%)	91.0	90.0	89.7
Additionally allowed (%)	7.6	9.0	9.3
Generously allowed (%)	1.4	1.0	1.0
Disallowed (%)	0.0	0.0	0.0

Cbz-Gly-OH (0.21 g, 1 mmol), preactivated into its mixed anhydride (as described above) with isobutyl chloroformate (0.14 ml, 1.05 mmol) and *N*-methylmorpholine (0.25 ml, 2.2 mmol) in anhydrous THF (10 ml), was added to the obtained pseudotripeptide hydrobromide. The suspension was stirred overnight and then evaporated to dryness. The residue was treated with ethyl acetate (25 ml) and acidified with 4 M HCl/dioxane. The organic layer was washed with brine (10 ml) and dried over Na_2SO_4. After removal of the solvent *in vacuo* the residue was redissolved in anhydrous dichloromethane (3 ml), treated with bromotrimethylsilane (2.64 ml, 20 mmol) and stirred for three days. Evaporation of volatile components gave the residue that was hydrolyzed overnight with water and concentrated HCl (2 ml and 5 ml added after 1 h, respectively). Final concentration under reduced pressure gave a sample for HPLC. The target tetrapeptide Gly-Glyψ[P(O)(OH)CH_2]-Gly-Gly-OH **4** was purified by two repetitive steps on an HPLC isocratic water gradient: $t=0$ min (0% B), $t=12$ min (0% B). R_t, 8.7 min. Yield, 15%. ^{31}P NMR (121.50 MHz, ^2H_2O): δ 45.83. ^{1}H NMR (300.13 MHz): δ 2.06 (m, 2H, PCH_2), 2.62 (m, 2H, PCH_2CH_2), 3.68 (d, $J=9.0$ Hz, 2H, NCH_2P), 3.94, 4.08 (s each, 2H and 2H, 2×CH_2).

Crystallization and data collection

For crystallization, $LytM_{185\text{-}316}$ was dialyzed against buffer A and concentrated to 12 mg/ml. Crystals were grown by the sitting-drop, vapour-diffusion method at 21 °C. Then 1.5 µl of protein solution was mixed with 1.5 µl of reservoir solution and equilibrated against reservoir buffer. Three different crystal forms were obtained.

The first crystals were grown with reservoir buffer containing 0.1 M Tris–HCl, 2 M mono-ammonium dihydrogen phosphate (final pH 4.5) and belonged to the spacegroup *P*3(2)21. For cryoprotection, crystals were soaked for 20 s in the mixture containing reservoir buffer, water and 2,3-butanediol (2:2:1; by vol.).

Another crystal form of native $LytM_{185\text{-}316}$ could be obtained by mixing 1.5 µl of reservoir buffer containing 30% polyethylene glycol 8000, 0.2 M ammonium sulphate, 0.1 M sodium cacodylate (final pH 6.8), 1.5 µl of concentrated protein and 0.3 µl of 1 M sodium acetate. These crystals belonged to spacegroup *P*2(1)2(1)2(1) and they could be flash-cryocooled after a short incubation in the mixture of reservoir buffer and 2,3-butanediol (9:1, v/v). The datasets of both crystal forms were collected at beamline BW6, DESY in Hamburg.

The crystals of the complex of $LytM_{185\text{-}316}$ with L(+)-tartrate were grown from reservoir buffer containing 30% polyethylene glycol 8000, 0.2 M L(+)-tartrate and 0.1 M Mes (final pH 6.5). As this screen was used in attempt to get the complex with phosphinic acid analogue, the compound was also present at 20 mM concentration in the drop. Crystals grew for two months at room temperature, and could be flash-cryocooled without buffer exchange. They were measured in-house on a Rigaku rotating anode generator, diffracted to 1.5 Å with excellent statistics and belonged to the tetragonal system, spacegroup *P*4(1).

Structure determination and refinement

The diffraction data for the trigonal and tetragonal crystal forms were processed with DENZO/SCALEPACK,[28] and the data for the orthorhombic crystal form were integrated with MOSFLM[29] and scaled with SCALA.[29] In all three crystal forms, the asymmetric units contained two protein molecules. Structures were solved with MOLREP,[30] using either residues 186–314 of the full-length LytM structure (PDB accession code 1QWY) or the structure of $LytM_{185\text{-}316}$ in a previously solved crystal form as the search model. Structures were improved iteratively by manual model building, water picking with ARP/WARP[31] and refinement with REFMAC5.[32] NCS restraints were applied in the early stages of model improvement only. The final refinement for all three crystal forms was done with individual isotropic *B*-factors, but monomers were assigned to separate TLS groups. In the case of the *P*3(2)21 crystal form, a subtle violation of the *P*3(2)21 symmetry, which is not apparent in the diffraction data, was noticed. The treatment of this complication as either twinning or as a complicated case of multiple conformations is described in the Supplementary Data. Data collection and refinement statistics for all three crystal forms are summarized in Table 1.

Protein Data Bank accession codes

The atomic coordinates and structure factors have been deposited in the Protein Data Bank, Research Collaboratory for Structural Bioinformatics, Rutgers University, New Brunswick, NJ† with accession codes 2B44 for the *P*3(2)21 form, 2BOP for the *P*2(1)2(1)2(1) form and 2B13 for the *P*4(1) form.

Acknowledgements

We thank Dr Izabela Sabala and Sergey G. Odintsov for help and enzyme preparations, Rafal Klajn for his contributions in the early stages of the project, Professor Hans Bartunik for generous allocation of beamtime on BW6 (DESY, Hamburg) and Dr Gleb Bourenkov for help with data collection. This work was supported by the Deutsche Forschungsgemeinschaft DFG ("Proteolyse in Prokaryonten: Kontrolle und regulatorisches Prinzip", BO1733/1-1), by the European Communities, specific RTD programme "Quality of Life and Management of Living Resources", QLRT-2001-01250, "Novel non-antibiotic treatment of staphylococcal diseases" and by the Polish Ministry of Scientific Research and Information Technology (MNiI, decisions 1789/E-529/SPB/5.PR UE/DZ 600/2002-2005, 158/E-338/SPB/5.PR UE/DZ 19/2003 and KO89/ PO4/ 2004). M.B thanks EMBO and HHMI for Young Investigator support.

Supplementary Data

Supplementary data associated with this article can be found, in the online version, at doi:10.1016/j.jmb.2005.09.082

References

1. Bochtler, M., Odintsov, S., Marcyjaniak, M. & Sabala, I. (2004). A common catalytic core in lysostaphins, D-alanyl-D-alanine carboxypeptidase and sonic hedgehog. *Protein Sci.* **13**, 854–861.
2. Marcyjaniak, M., Odintsov, S. G., Sabala, I. & Bochtler, M. (2004). Peptidoglycan amidase MepA is a LAS metallopeptidase. *J. Biol. Chem.* **279**, 43982–43989.
3. Breece, M. B., Costello, A., Bennett, B., Sigdel, T. K., Matthews, M. L., Tierney, D. L. & Crowder, M. W. (2005). A five-coordinate metal center in Co(II)-substituted VanX. *J. Biol. Chem.* **280**, 11074–11081.
4. Bussiere, D. E., Pratt, S. D., Katz, L., Severin, J. M., Holzman, T. & Park, C. H. (1998). The structure of VanX reveals a novel amino-dipeptidase involved in mediating transposon-based vancomycin resistance. *Mol. Cell*, **2**, 75–84.
5. Dideberg, O., Charlier, P., Dive, G., Joris, B., Frere, J. M. & Ghuysen, J. M. (1982). Structure of a Zn^{2+}-containing D-alanyl-D-alanine-cleaving carboxypeptidase at 2.5 Å resolution. *Nature*, **299**, 469–470.
6. Brandt, J. J., Chatwood, L. L., Yang, K. W. & Crowder, M. W. (1999). Continuous assay for VanX, the D-alanyl-D-alanine dipeptidase required for high-level vancomycin resistance. *Anal. Biochem.* **272**, 94–99.
7. Charlier, P., Wery, J. P., Dideberg, O. & Frère, J. (2004). *Streptomyces albus* G D-Ala-D-Ala carboxypeptidase. In *Handbook of Metalloproteins* (Messerschmidt, A., Bode, W. & Cygler, M., eds), vol. 3, pp. 164–175, John Wiley & Sons, Ltd, Chichester.
8. Kessler, E., Safrin, M., Gustin, J. K. & Ohman, D. E. (1998). Elastase and the LasA protease of Pseudomonas aeruginosa are secreted with their propeptides. *J. Biol. Chem.* **273**, 30225–30231.
9. Kokai-Kun, J. F., Walsh, S. M., Chanturiya, T. & Mond, J. J. (2003). Lysostaphin cream eradicates Staphylococcus aureus nasal colonization in a cotton rat model. *Antimicrob. Agents Chemother.* **47**, 1589–1597.
10. Odintsov, S., Sabala, I., Marcyjaniak, M. & Bochtler, M. (2004). Latent LytM at 1.3 Å resolution. *J. Mol. Biol.* **335**, 775–785.
11. Ramadurai, L. & Jayaswal, R. K. (1997). Molecular cloning, sequencing, and expression of lytM, a unique autolytic gene of *Staphylococcus aureus*. *J. Bacteriol.* **179**, 3625–3631.
12. Schleifer, K. H. & Kandler, O. (1972). Peptidoglycan types of bacterial cell walls and their taxonomic implications. *Bacteriol. Rev.* **36**, 407–477.
13. Collinsová, M. & Jiráček, J. (2000). Phosphinic acid compounds in biochemistry, biology and medicine. *Curr. Med. Chem.* **7**, 629–647.
14. Brennan, S. & Cowan, P. L. (1992). A suite of programs for calculating X-ray absorption, reflection and diffraction performance for a variety of materials at arbitrary wavelengths. *Rev. Sci. Instrum.* **63**, 850.
15. Harding, M. M. (2002). Metal-ligand geometry relevant to proteins and in proteins: sodium and potassium. *Acta Crystallog. sect. D*, **58**, 872–874.
16. Browner, M. F., Smith, W. W. & Castelhano, A. L. (1995). Matrilysin-inhibitor complexes: common themes among metalloproteases. *Biochemistry*, **34**, 6602–6610.
17. Cuniasse, P., Devel, L., Makaritis, A., Beau, F., Georgiadis, D., Matzari, M. *et al*. (2005). Future challenges facing the development of specific active-site-directed synthetic inhibitors of MMPs. *Biochimie*, **87**, 393–402.
18. Wang, R., Lu, Y. & Wang, S. (2003). Comparative evaluation of 11 scoring functions for molecular docking. *J. Med. Chem.* **46**, 2287–2303.
19. Quin, D. C. & Robinson, R. (1943). Attempts to find new antimalarials. *J. Chem. Soc. Perkin Trans.* **18**, 555–557.
20. Fitch, S. J. (1964). Synthesis of hypophosphite esters from orthocarbonyl compounds. *J. Am. Chem. Soc.* **86**, 61–64.
21. Cristau, H. J., Coulombeau, A., Genevois-Borella, A. & Pirat, J. L. (2001). A convenient one-pot synthesis of phosphino-dipeptide analogs. *Tetrahedron Letters*, **42**, 4491–4494.
22. Cristau, H. J., Coulombeau, A., Genevois-Borella, A., Sanchez, F. & Pirat, J. L. (2002). Preparation of phosphinodipeptide analogs as building blocks for pseudopeptides synthesis. *J. Organomet. Chem.* **643–644**, 381–391.

† http://www.rcsb.org

23. Baylis, E. K., Campbell, C. D. & Dingwall, J. G. (1984). 1-Aminoalkylphosphonous acids. Part 1. Isosteres of the protein amino acids. *J. Chem. Soc. Perkin Trans. 1*, 2845–2853.
24. Buchardt, J., Ferreras, M., Krog-Jensen, C., Delaissé, J. M., Foged, N. T. & Meldal, M. (1999). Phosphinic peptide matrix metalloproteinase-9 inhibitors by solid-phase synthesis using a building block approach. *Chem. Eur. J.* **5**, 2877–2884.
25. Vassiliou, S., Mucha, A., Cuniasse, P., Georgiadis, D., Lucet-Levannier, K., Beau, F. *et al*. (1999). Phosphinic pseudo-tripeptides as potent inhibitors of matrix metalloproteinases: a structure-activity study. *J. Med. Chem.* **42**, 2610–2620.
26. Grembecka, J., Mucha, A., Cierpicki, T. & Kafarski, P. (2003). The most potent organophosphorus inhibitors of leucine aminopeptidase. Structure-based design, chemistry and activity. *J. Med. Chem.* **46**, 2641–2655.
27. Mucha, A., Pawelczak, M., Hurek, J. & Kafarski, P. (2004). Synthesis and activity of phosphinic tripeptide inhibitors of cathepsin C. *Bioorg. Med. Chem. Letters*, **14**, 3113–3116.
28. Otwinowski, Z. & Minor, W. (1997). Processing of X-ray diffraction data collected in oscillation mode. *Methods Enzymol.* **276**, 307–326.
29. Leslie, A. W. G. (1990). *Crystallographic Computing*, Oxford University Press, Oxford.
30. Vagin, A. & Teplyakov, A. (2000). An approach to multi-copy search in molecular replacement. *Acta Crystallog. sect. D*, **56**, 1622–1624.
31. Morris, R. J., Perrakis, A. & Lamzin, V. S. (2003). ARP/wARP and automatic interpretation of protein electron density maps. *Methods Enzymol.* **374**, 229–244.
32. Murshudov, G. N., Vagin, A. A. & Dodson, E. J. (1997). Refinement of macromolecular structures by the maximum-likelihood method. *Acta Crystallog. sect. D*, **53**, 240–255.

Edited by R. Huber

(Received 5 July 2005; received in revised form 23 September 2005; accepted 27 September 2005)
Available online 18 October 2005